TECHNICAL NOTE

FLOW FIELD SIMULATIONS OVER REENTRY MODULES AT HIGH SPEED

R. C. Mehta*

Abstract

Reentry capsule configurations significantly differ from each other due to entry conditions and mission requirements. This paper describes numerical simulations of the viscous flow over the Beagle and the OREX (Orbital Reentry EXperiments) configurations for freestream Mach numbers in the range of 1.2 - 5.0. The flow fields over the reentry modules are obtained by solving time-dependent axisymmetric compressible laminar Navier-Stokes equations. The fluid mechanics equations are discretized in spatial coordinates employing a finite volume method, which reduces the governing equations to semi-discretized ordinary differential equations. Temporal integration is carried out using a two-stage Runge-Kutta time-stepping scheme. A local time-stepping is employed to get the steady state solution. The numerical simulation is performed on a single-block structured grid. The flow field features around the reentry capsules such as bow shock wave, sonic line, expansion fan and recirculation flow in the base-shell region are well captured by the present numerical computation. The effects of the geometrical parameters of the module, such as aspect ratio, frontal segment bluntness, fore body cone angle and shoulder rounding radius on the wake throat width, distance from the wake throat to the base of the model, flow departure angle and aerodynamic drag are analyzed using the numerically simulated flow field.

Introduction

The primary design consideration of reentry capsules requires large spherical nose radius of their fore-body that gives high aerodynamic drag and a short body length for reducing the total structure weight and the ballistic coefficient. The fore-body shape of reentry capsules can be selected by either employing a spherical cap, or a combination of spherical nose with cone, or a spherical blunt cone/flare configuration. To ensure the deployment of the parachute in the transonic region, the flow field past the capsule must be known at supersonic speeds. The flow field in the wake region of a reentry capsule is complex due to the expansion at the shoulder and the base-shell. The bow shock wave is detached from the blunt fore-body and is having a mixed subsonic-supersonic region between them. The surface pressure distribution, the location of the sonic line and the shock stand-off distance on the spherical cap have been analytically calculated at very high speeds with an adiabatic index close to unity which gives a singular point at 60° from the stagnation point [1, 2]. The flow-field over the reentry capsule is further complicated by the presence of a corner at the shoulder and the base shell of the reentry module. Experimental investigation of various types of cone-segment bodies and spheres of Russian reentry capsules were carried out by Bedin et al. [3] in a pressure-tight ballistic range, with the specific heats ratio between 1.14 - 1.67, Mach number varying from 0.5 - 10, and Reynolds number based on the base diameter varying from 2.5×10^5 - 5.0×10^6. Fig.1 depicts the geometrical parameters of the Russian reentry modules tested in the ballistic facility. They observed that the static aerodynamic characteristic errors at ballistic range vary significantly depending on the experimental method, techniques used for processing results, and parameters of the models and medium.

The flow is curved in the direction of the freestream on the spherical cap of the capsule and the pressure from the shock wave to the body surface equals the centrifugal force due to the curvature of the flow [4]. The pressure coefficient behind the bow shock wave depends on the surface slope of the fore body of the reentry module. The pressure relief due to the curvature depends on the local density, the velocity, and the radius of the curvature of the spherical cap. The shape of the bow shock wave and the detachment distance depend on the geometry of the reentry capsule and on the freestream Mach number [5]. The

* School of Mechanical and Aerospace Engineering, Nanyang Technological University, Singapore 639 798
Email : atulm@md4.vsnl.net.in
Manuscript received on 14 Aug 2009; Paper reviewed, revised and accepted as a Technical Note on 07 Dec 2009

analytical approach to study the high speed flow past the blunt body is considerably difficult and complex [6]. The flow field features over the reentry capsules can be delineated through numerical simulation at high speeds. The significant flow features over the reentry capsule at high speeds can be described as follows. In the fore-body region, the fluid decelerates through the bow shock wave depending upon the trajectory conditions. At the shoulder of the capsule, the flow turns and expands rapidly, and the boundary layer detaches, forming a free shear layer that separates the inner re-circulating flow behind the base from the outer flow field. The latter is recompressed and turned back to freestream direction, first by the so-called lip shock, and further downstream by recompression shock. At the end of the re-circulating flow past the neck, the shear layer develops in the wake trail. A complex inviscid wave structure often includes a lip shock and wake trail. Fig.2 shows schematic features of the flow field over a typical reentry module.

A large number of computational fluid dynamics simulations [7-10] have been performed for aerobraking and reentry capsules. Allen and Cheng [11] have carried out the numerical solution of Navier-Stokes equations in the near wake region of the reentry module, which confirms the mechanism of flow separation as, observed experimentally [12]. Base drag represents the loss in recovery of pressure over the base of the capsule [13]. The supersonic and hypersonic laminar flow over a slender cone has been numerically calculated by Tai and Kao [14]. A summary of developments relating to the base pressure prediction is reported in the review paper of Lamb and Oberkampf [15]. An aerodynamic analysis of the Commercial Experiment Transport (COMET) reentry capsule carried out by Wood et al. [16] by utilizing the laminar thin layer Navier-Stokes equations flow solver LAURA. The flow field past a blunt and short reentry capsule has been analyzed in order to understand the mechanism of the instability at supersonic speeds due to decay of base pressure [17]. Yamamoto et al. [18] have computed flow field over the OREX reentry module in conjunction with the in-depth thermal analysis of the thermal protection system and the results were compared with the flight data. Tam [19] has used LUSGS implicit scheme for flow computation over On-Axis Biconic and Aeroassist Flight Experiment (AFE) reentry vehicles. Liever et al. [20] solved the flow field over Beagle reentry capsule. The flow field and the heat flux computation over the Mars pathfinder vehicle has been numerically carried out by Haas and Venkatapathy [21] along with the fore body and wake flow structure during atmospheric entry of the spacecraft.

The above literature survey shows that the fore-body shape of the reentry capsules can be classified as either using a spherical cap, or a combination of the spherical cap with a cone. In the present work, numerical studies were undertaken for freestream supersonic Mach numbers of 1.2 - 5.0. The numerical simulation to solve the axisymmetric laminar compressible unsteady Navier-Stokes equations is by employing a two-stage Runge-Kutta time-stepping scheme. The numerical scheme is second order accurate in space. The numerical simulation is carried out on a mono-block structured grid. Surface pressure and fore-body aerodynamic drag on the Beagle and the OREX (Orbital Reentry EXperiments) configurations are computed numerically, which will give a systematic understanding of the flow features at supersonic Mach numbers and varying geometrical parameters of the reentry modules. The objective of the present note is to provide an insight into the flow field such as the separated zone and vortex formation in the base region of two different types of reentry modules. The effects of the geometrical parameters of the module, such as the length to diameter ratio (aspect ratio), spherical cap radius, shoulder rounding radius, fore-body segment cone angle and back shell inclination angle on the flow field over the capsule, will provide a useful input for the specific mission requirement of selecting the reentry module.

Governing Equations

The time-dependent axisymmetric compressible Navier-Stokes governing equations can be written in the following strong conservation form as

$$\frac{\partial \boldsymbol{U}}{\partial t} + \frac{\partial \boldsymbol{F}}{\partial x} + \frac{1}{r}\frac{\partial (r\boldsymbol{G})}{\partial r} = \frac{\boldsymbol{H}}{r} \qquad (1)$$

where

$$\mathbf{U} = [\rho, \quad \rho u, \quad \rho v, \quad \rho e]^T$$

$$\mathbf{F} = \left[\rho u, \ \rho u^2 - \sigma_{xx}, \ \rho uv - \sigma_{xr}, \ (\rho e - \sigma_{xx})u - \sigma_{xr}v + q_x\right]^T$$

$$\mathbf{G} = \left[\rho v, \ \rho uv - \sigma_{xr}, \ \rho v^2 - \sigma_{rr}, \ (\rho e - \sigma_{rr})v - \sigma_{rx}u + q_r\right]^T$$

$$\mathbf{H} = \left[0, \quad 0, \quad \sigma_{+}, \quad 0\right]^T$$

where **U** is the conservative variables in vector form, **F** and **G** are flux vectors in x and r direction, respectively. u and v are velocity components. p and ρ are pressure and density of the fluid, respectively, and e is the specific energy. **H** is the source vector. σ_{xx}, σ_{rr}, σ_{xr}, and σ_{+} are components of the stress vector, while q_x and q_r are components of the heat flux vector. The viscous and heat flux terms in the equations become

$$\sigma_{xx} = -\frac{2}{3}\mu\nabla . U + 2\mu\frac{\partial u}{\partial x}$$

$$\sigma_{rr} = -\frac{2}{3}\mu\nabla . U + 2\mu\frac{\partial v}{\partial r}$$

$$\tau_{xr} = \mu\left(\frac{\partial u}{\partial r} + \frac{\partial v}{\partial x}\right)$$

$$\sigma_{+} = -p - \mu\frac{2}{3}\nabla . U + 2\mu\frac{v}{r}$$

$$\nabla . U = \frac{\partial u}{\partial x} + \frac{\partial v}{\partial r} + \frac{v}{r}$$

$$q_x = -\frac{C_p\mu}{P_r}\frac{\partial T}{\partial x}$$

$$q_r = -\frac{C_p\mu}{P_r}\frac{\partial T}{\partial x} \qquad (2)$$

where C_p is specific heat at constant pressure, U is the mean stream velocity, Pr is Prandtl number and is taken a constant value of 0.72. The coefficient of molecular viscosity μ is calculated using Sutherland's law. The temperature is related to pressure and density by the perfect gas equation of state as

$$p = \rho(\gamma - 1)\left[e - \frac{1}{2}(u^2 + v^2)\right] \qquad (3)$$

where γ is ratio of specific heats. The flow is assumed to be laminar, which is consistent with the numerical simulation of [14, 16, 22].

Numerical Algorithm

The numerical algorithm uses a finite volume discretization technique. The computational domain is divided into a number of quadrilateral cells. The conservative variables **U** within each cell are calculated from their average values at the cell centre. The flux vectors **F**, **G**, and **H** are computed on each side of the cell [23]. Spatial and temporal terms are decoupled using the method of lines. A system of ordinary differential equations in time is obtained after integrating Eq. (1) over a computational cell and summing the flux vector on each side of the cell. The finite volume code constructed in this manner reduces to a central-difference scheme and is second-order accurate in space provided that the mesh is smooth enough. Temporal integration is done by the multi-stage method [24], based on the Runge-Kutta scheme. This method requires an additional artificial dissipation term to prevent odd-even decoupling and to control numerical oscillations in the vicinity of severe pressure gradients. Fourth-order dissipation is added everywhere in the flow domain where the solution is smooth but is switched off in the region of shock waves. The term involving the second-order difference is switched on to damp numerical oscillations near the shock waves. The scheme is stable for a Courant number less than or equal to 1. Local time steps are used to accelerate to a steady-state solution by setting the time step at each point to the maximum value allowed by the local Courant-Friedrichs-Lewy (CFL) condition.

Initial and Boundary Conditions

The initial conditions corresponding to the supersonic freestream Mach numbers are given in Table-1. The boundary conditions are as follows. All variables are extrapolated at the outer boundary, and a no-slip condition is used as wall boundary condition. An isothermal wall condition is considered for the surface of the reentry configuration. The wall temperature is prescribed as 231K. A symmetry condition is applied on the centre line ahead and downstream of the reentry capsule.

Geometrical Details of the Reentry Modules

The dimensional details of the Beagle and the OREX modules, shown in Fig.3, are of axisymmetric designs. The fore-body of the Beagle has a cone angle $\alpha_N = 60°$ with a maximum diameter D = 3.0 m. The Beagle capsule has a spherical blunt nose radius of R=1.39 m, and a shoulder radius of R_C = 0.029 m. The back shell has an inclination angle $\alpha_B = 43.75°$ relative to the vehicles axis of symmetry as depicted in Fig.3(a). The overall length of the module is L = 1.665 m and the length to diameter ratio is 0.555.

The OREX has a spherical nose cap and a conical section of diameter D = 3.40 m with $\alpha_N = 50°$ as depicted

in Fig. 3(b). The OREX capsule has a spherical blunt nose radius of R = 1.35 m. The outer edge of the module has a rounded edge of R_C = 0.01m and the rear of the module is made up of a conical panel with $\alpha_B = 75°$ as measured from the clockwise direction. The overall length of the OREX module is L = 1.508 m and the aspect ratio is 0.443.

Computational Grid

One of the controlling factors for the numerical simulation is a proper grid arrangement. In order to initiate the numerical simulation of the flow along the reentry module, the physical space is discretized into non-uniform spaced grid points. These body-oriented grids are generated using a finite element method in conjunction with homotopy scheme [25, 26]. The typical computational space of the reentry module is defined by a number of grid points in a cylindrical coordinate system. Using these surface points as the reference nodes, the normal coordinate is then described by exponentially stretched grid points, extending onwards up to an outer computational boundary. The stretching of the grid points in the normal direction is obtained using the exponentially stretching relation. These grids are generated in an orderly manner. Grid independence tests [27] were carried out, taking into consideration the effect of the computational domain, the stretching factor to control the grid density near the wall, and the number of grid points in the axial and normal directions. A rigorous grid refinement study with successive doubling of the number of cells in each direction is carried out. The present numerical analysis is carried out on 132 x 62 grid points. Fig.4 displays the enlarged view of the mono-block structured grid over the OREX reentry configurations. This spatial resolution is adequate for fine resolution of the boundary layer and the complex flow field. The finer mesh near the wall helps to resolve the viscous effects. The coarse grid helps in reducing the computer time. The grid-stretching factor is selected as 5, and the outer boundary of the computational domain is maintained as 1.5 - 2.5 times the maximum diameter of the reentry module. In the downstream direction the computational boundary is about 6 - 9 times the diameter of the module, D. The nature of the flow fields examined in this study is generally quasi-steady [28]. The grid arrangement is found to give a relative difference of about ±1.5% in the computation of drag coefficient. The convergence criterion is based on the difference in density values ρ at any of the grid points, between two successive iterations $| \rho^{n+1} - \rho^{n} | \leq 10^{-5}$ where n is time-step counter.

Results and Discussion

The numerical procedure mentioned in the previous section is applied to simulate the flow field over the Beagle and the OREX reentry capsules for freestream Mach numbers in the range of 1.2 - 5.0, and for freestream Reynolds numbers ranging from 1.967×10^7 - 8.198×10^7/m, based on the initial conditions as given in Table-1.

Table-1 : Initial Conditions

M_∞	U_∞, m/s	P_∞, Pa	T_∞, K
1.2	351	4519	210
1.4	409	4501	21
2.0	596	2891	219
3.0	903	2073	224
5.0	1532	1238	232

Flow Characteristics

Figures 5 and 6 show the close-up view of the velocity vector plots over the Beagle and the OREX at M_∞ = 1.2 - 5.0. It can be seen from the vector plots that the bow shock wave follows the body contour relatively close to the fore-body. A separated flow can be observed in the base region of the reentry capsules. The flow around the capsule is divided into two regions inside and outside of the recirculation, and the shear layer separates the regions. The flow field is very complex because of the back-shell geometry of the module. The wake flow field, immediately behind the capsule base, exhibits vortex flow behavior. The formation of the bow shock wave on the fore-body of the OREX capsule depends on geometrical parameters such as the spherical cap radius and the apex cone angle, and the value of the freestream Mach number. The bow shock wave moves close to the fore-body with the increasing freestream Mach number, i.e. stand-off distance between the bow shock wave and the fore-body decreases with increasing of the freestream Mach number. The approaching boundary layer separates at the corner and the free shear layer is formed in the wake region. The wake flow also shows a vortex attached to the corner with a large recirculation, which depends on the spherical nose radius, fore-body segment cone angle α_N, back-shell inclination angle α_B and freestream Mach number M_∞. The separation point moves downstream from the shoulder towards the base with increasing M_∞. Similar flow field features were observed in the analysis of the bulbous payload shroud of the heat shield of the launch vehicle [29].

Computed Mach contour plots around the Beagle and the OREX for M_∞ = 1.2 - 5.0 are depicted in Figs.7 and 8. The velocity vector plots show the formation of vortices at the corner region of the capsule for $M_\infty \leq 3$. Characteristic features of the flow field around the blunt body at supersonic Mach numbers, such as the bow shock wave ahead of the capsule, the wake, and the recompression shock waves emanating from the shoulder point, are seen in the Mach contour plots. The bow shock wave following the body contour and the fore-body is entirely subsonic up to the corner point of the Beagle and the OREX modules, where the sonic line is located. The Mach contour plots reveal many interesting flow features of the reentry capsule. The flow expands at the base corner and is followed by the recompression shock downstream of the base, which realigns the flow. The flow then develops in the trailing wake. As observed in the figures, vortices are generated at the capsule surface and are then moving, changing location with the freestream Mach number. We can also observe the strong vortex flow over the shoulder of the capsule at freestream Mach number 1.2 and 2.0. The flow may become unsteady at supersonic Mach numbers due to the formation of the vortices. Note, however, that the use of a fixed CFL number in the present numerical flow simulation leads to a local time step size, which differs throughout the flow domain. All the essential flow field characteristics over the reentry body are well captured by the present numerical algorithm in conjunction with a single block structured grid arrangement. At the shoulder, the flow turns and expands rapidly, and boundary layer detaches, forming a free shear layer that separates the inner re-circulating region behind the base flow from the outer flow field as visualized in the velocity vector plots. At the end of the recirculation past the neck, the shear layer develops in the wake trails. It is important to mention here that a complex inviscid wave structure often includes a lip shock (associated with the corner expansion) and a wake shock (adjacent to the shear layer confluence). The corner expansion process is a modified Prandtl-Mayer pattern distorted by the presence of the approaching boundary layer. As the flow breaks from the base plane it is brought to the base pressure by a weak shock wave known as the lip shock downstream from the lip shock, the free shear layer regions to form. A free shear layer (in contrast to a boundary layer) is characterized by the nearly zero velocity derivatives (shear stresses) at each edge of the layer. It can be seen from the contour plots that a strong vortex flows at the shoulder. The rapid expansion around the fore-body corners produces high Mach numbers in the outer inviscid region of the wake. The flow field depends on the geometrical parameters as well as freestream Mach number. The separation point in the base region moves down stream as the freestream Mach number increases. Fig.9 shows the presentation of geometrical parameters and wake region flow field based on the velocity vector and the Mach contour plots. The flow departure angle β is about 30° at Mach 1.2 for the Beagle module. The angle β becomes about -9° for the Mach number 5. A similar behaviour for the flow departure was found by Bedin et al. [3]. The ratio of wake throat width h to diameter of the capsule D varies in between 1.0 to 0.25. The ratio of wake throat location L_c to the diameter of the model D is in the decreasing trend as can be seen in the Mach contour plots. It varies from 2 to 0.5.

Surface Pressure Distribution

Figures 10 and 11 display the pressure coefficient $\left[C_p = 2\{ (p/p_\infty) - 1\}/(\gamma M_\infty^2) \right]$ variation along the model surface for the Beagle and the OREX for M_∞ = 1.2 - 5.0. The s/D = 0 location is the stagnation point, where s represents the surface arc distance length and D is the maximum diameter of the capsule. The variation of the pressure coefficient on the spherical region decreases gradually for the Beagle and the OREX capsules whereas in the conical region of the OREX it remains constant. The pressure coefficient falls on the sphere-cone junction and remains constant over the cone for the OREX and the sonic point moves to the corner of the blunt bodies and affects the pressure distribution throughout the subsonic flow. In the case of the OREX with α_N = 50°, the pressure coefficient shows over-expanded flow. A sudden drop of the pressure coefficient is observed on the shoulder of the module followed by the negative pressure coefficient variation in the base region. A low pressure is formed immediately downstream of the base, which is characterized by a low speed re-circulating flow region, which can be attributed to the fill up of the growing space between the shock wave and body. In the base region, the pressure coefficient is decreasing with increasing freestream Mach number. The effect of the corner radius on the pressure coefficient is higher. The C_P variation depends on the geometry of the capsules. The value of C_P in the back-shell region of the OREX is similar with the Beagle module. A low pressure is observed immediately downstream of the base which is characterized by a low-speed re-circulating flow region, which can be attributed to the fill-up of the growing space between the shock wave and the reentry module. The fore-body of the Beagle capsule is experiencing higher pressure as compared to the OREX module. This can be attributed to the fore-body semi-cone

angle α_N = 60° for the Beagle whereas it is 50° for the OREX.

Pressure drag is calculated by integrating the pressure distribution on the body surface excluding the base of the capsule and can be expressed as

$$C_D = \frac{2\pi C_p r_i \int \tan\theta_i \, dx}{A_{max}} \quad (4)$$

where r and θ are the local radius and local inclination angle in the x-direction of station *i*. A_{max} is the maximum area of the capsule. The forebody aerodynamic drag C_D is given in Table-2 for the Beagle and the OREX for M_∞ = 1.2 - 5.0. For the calculation of C_D the reference area is the maximum cross-sectional area of the capsule. The base pressure is somewhat constant. The value of C_D is higher for the OREX capsule as compared to the Beagle, at M_∞ = 1.2 and 1.4. Then, the C_D becomes higher for the Beagle capsule as compared to the OREX module at high Mach numbers. Thus the value of C_D depends on the fore-body geometry as well as freestream Mach numbers which influences the flow expansion over the shoulder of the capsule.

Table-2 : Fore Body Aerodynamic Drag Coefficient

Capsules	M_∞=1.2	M_∞=1.4	M_∞=2.0	M_∞=3.0	M_∞=5.0
Beagle	1.59	1.58	1.54	1.47	1.42
OREX	1.79	1.77	1.50	1.30	1.16

The skin friction coefficient C_f along the surface of the capsule is computed using following relation

$$C_f = -\frac{\mu \left|\frac{\partial u}{\partial r}\right|_{wall}}{\frac{1}{2}\rho u_\infty^2} \quad (5)$$

Figures 12 and 13 depict the variation of C_f along the surface of the capsule with M_∞ as a parameter. C_f decreases with increasing M_∞ on the fore-body. A sudden drop in the skin friction coefficient is found at the shoulder of the capsule. This may be attributed to sudden expansion of the flow on the corner. Negative skin friction can be seen on the base, which is due to separated flow. The separation zone is found to be a function of M_∞ and the geometry of the base region of the capsule. In the base region of the Beagle, the skin friction coefficient variation in the wake region of the Beagle module is having oscillation which is due to the change of flow separation zone as also noticed in the velocity vector plots.

Figures 14 and 15 give the variation of wall heat flux Q_w over the Beagle and the OREX configurations, respectively. Both the reentry modules experience high wall heat flux in the fore-body region. The OREX configuration is having more wall heat flux in the base region as compared with the Beagle. The base region heat flux depends on the base region geometrical parameters. The base shell of the OREX is having a 75° inclination whereas the Beagle is having 43.75°. The base heat flux is about 2 - 5% of the stagnation point heat flux.

Conclusions

The flow field over the Beagle and OREX reentry capsules is computed by solving compressible laminar and time-dependent axisymmetric laminar Navier-Stokes equations. A single-block structured, axisymmetric, finite volume code solves the governing fluid dynamics equations using two-stage Runge-Kutta time stepping scheme with local time stepping in order to accelerate the convergence for obtaining a steady state solution. All the essential flow field features are fairly well captured such as the bow shock wave, expansion on the corner, recompression shock wave and recirculation flow in the base region. The flow field visualization of the separation region helps in a systematic understanding of the flow field features under various freestream Mach numbers. The effects of the module geometrical parameters, such as the aspect ratio, frontal segment bluntness, fore-body cone angle and the shoulder rounding radius on the wake throat width, distance from the wake throat to the base of the model, flow departure angle and aerodynamic drag are analyzed using the numerically simulated flow field on the reentry module.

Acknowledgement

The author expresses his sincere gratitude to the Referees for giving valuable suggestions toward the improvement of the present work.

References

1. Chester, W., "Supersonic Flow Past a Bluff Body with Detached Shock", Journal of Fluid Mechanics, 1956, 1, pp.353-365.

2. Freeman, N. C., "On the Theory of Hypersonic Flow Past Plane and Axially Symmetric Bluff Bodies", Journal of Fluid Mechanics, 1956, 1, pp.366-375.

3. Bedin, A. P., Mishin, G. I. and Chistyakova, M. V., "Experimental Investigation of the Aerodynamic Characteristics and Geometric Parameters of Flows about Blunted Bodies in Gases with Various Molecular Structures" in Gas Dynamics, Edited by Yu. I. Koptev, Nova Science Publishers, Inc. New York, 1992, pp. 39-67.

4. Lighthill, M. J. "Dynamics of a Dissociating Gas, Part 1: Equilibrium Flow", Journal of Fluid Mechanics, 1957, 2, pp.1-32.

5. Liepmann, H. W. and Roshko, A., "Elements of Gasdynamics" (Dover Publications Inc), First South Asian Edition, New Delhi, 2007.

6. Truitt, R. W., "Hypersonic Aerodynamics", The Ronald Press Co, New York, 1959.

7. Gnoffo, P. A., Price, J. M. and Braum, R. D., "On the Computation of Near Wake of Aero-brake Flow Field", AIAA paper 91-1371, June 1991.

8. Grasso, F. and Marinir, M., "Solution of Hypersonic Flows with Total Variation Diminishing Multigrid Technique", Computer and Fluids, 1995, 23 (5), pp.571-592.

9. Venkatapathy, E., Palmer, G. and Prabhu, D. K., "AFE Base Computations", AIAA Paper 91-1372, June 1991.

10. Osu, H., Abe, T., Ohnishi, Y., Sasoh, A. and Takayama, K., "Numerical Investigation of High Enthalpy Flow Generated by Expansion Tube", AIAA Journal, 2002, 40 (12), pp. 2423-2430.

11. Allen, J. S. and Cheng, S. I., "Numerical Solution of the Compressible Navier-Stokes Equations for the Near Wake", Physics of Fluids, 1970, 13 (1), pp.37-52.

12. Weinbaum, S., "Rapid Expansion of a Supersonic Boundary Layer and its Applications to the Near Wake", AIAA Journal, 1966, 4 (2), pp. 217-226.

13. Grasso, F. and Pettinelli, C., "Analysis of Laminar Near Wake Hypersonic Flow", Journal of Spacecraft and Rockets, 1995, 32 (6), pp. 970-980.

14. Tai, C-S. and Kao, A. F., "Navier-Stokes Solver for Hypersonic Flow Over a Slender Cone", Journal of Spacecraft and Rockets, 1994, 31 (1), pp. 215-222.

15. Lamb, J.P. and Oberkampf, W.L., "Review and Development of Base Pressure and Base Heating Correlations in Supersonic Flow", Journal of Spacecraft and Rockets, 1995, 32 (1), pp.8-23.

16. Wood, A. W., Gnoffo, P. A. and Rault, D. F. G., "Aerodyanmic Analysis of Commercial Experiment Transport Reentry Capsule", Journal of Spacecraft and Rockets, 1996, 33 (5), pp. 643-646.

17. Teramoto, S., Hiraki, K. and Fujii, K., "Numerical Analysis of Dynamic Stability of a Reentry Capsule at Transonic Speeds", AIAA Journal, 2001, 39 (4), pp. 646-653.

18. Yamamoto, Y. and Yoshioka, M., "CFD and FEM Coupling Analysis of OREX Aero-thermodynamic Flight Data", AIAA Paper 95-2087, 1995.

19. Tam, L. T., "LU-SGS Implicit Scheme for Entry Vehicle Flow Computation and Comparison with Aerodynamic Data", AIAA Paper 92-2671 CP, 1992.

20. Liever, P. A., Habchi, S. D., Burnell, S. I. and Lingard, J. S., "Computational Fluid Dynamics Prediction of the Beagle-2 Aerodynamic Data Base", Journal of Spacecraft and Rockets, 2003, 40 (5), pp. 632-638.

21. Haas, B. L. and Venkatapathy, E., "Mars Path Finder Computations Including Base Heating Predictions", AIAA Paper 95 2086, 1995.

22. Mehta, R. C., "Computation of Flow Field Over Reentry Capsules at Supersonic Mach Numbers", Computational Fluid Dynamics Journal, 2004, 13(3), pp.585-596.

23. Peyret, R. and Viviand, H., "Computational Methods for Fluid Flow", Springer-Verlag, New York, 1993.

24. Jameson, A., Schmidt, W. and Turkel, E., "Numerical Solution of Euler Equations by Finite Volume Methods using Runge-Kutta Time-stepping Schemes", AIAA Paper 81-1259, 1981.

25. Shang, J. S., "Numerical Simulation of Wing-fuselage Aerodynamic Interference", AIAA Journal, 1984, 22 (10), pp. 1345-1353.

26. Mehta, R.C., "A Quasi-three-dimensional Automatic Grid Generation Method", Proceedings of 25th National and International Conference on Fluid Mechanics and Fluid Power, Indin Institute of Techmology, Delhi, 1998, pp.89-98.

27. Mehta, R.C., "Numerical Analysis of Aerodynamic drag Coefficient for Various Reentry Configurations at High Speed", AIAA Paper 2006-3173, June 2006.

28. Mehta, R.C., "Numerical Simulation of Supersonic Flow Past Reentry Capsules", Shock Waves, 2006, 15 (1), pp. 31-41.

29. Mehta, R.C., "Flowfield over Bulbous Heat Shield in Transonic and Low Supersonic Speeds", Journal of Spacecraft and Rockets, 1998, 35 (1), pp.102-105 and also AIAA Paper 97-2256, 1997.

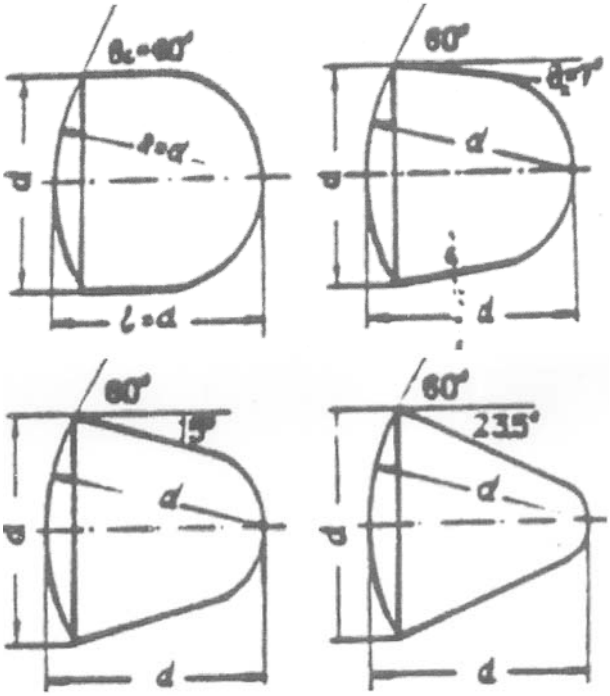

Fig.1 Geometrical Details of the Russian Reentry Capsules

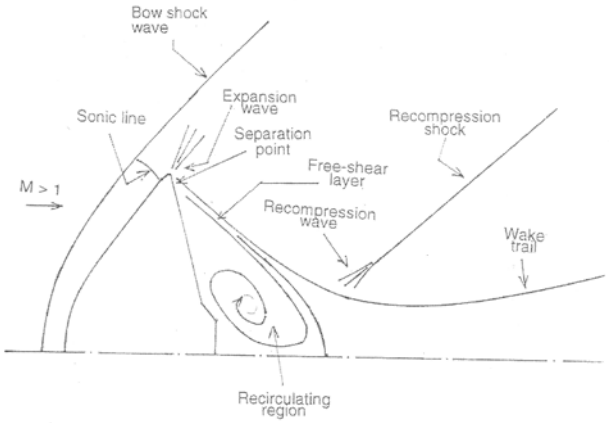

Fig.2 Presentation of Flow Features Over Reentry Body at Supersonic Speeds

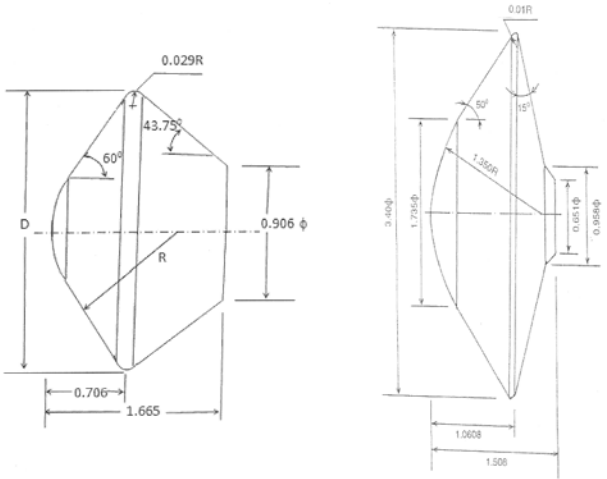

(a) Beagle (b) OREX

Fig.3 Geometrical Details of the Reentry Capsules

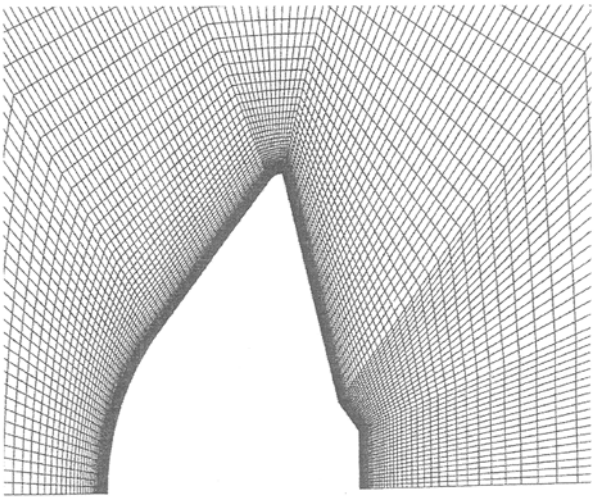

Fig.4 Enlarged View of Computational Grid OREX Module

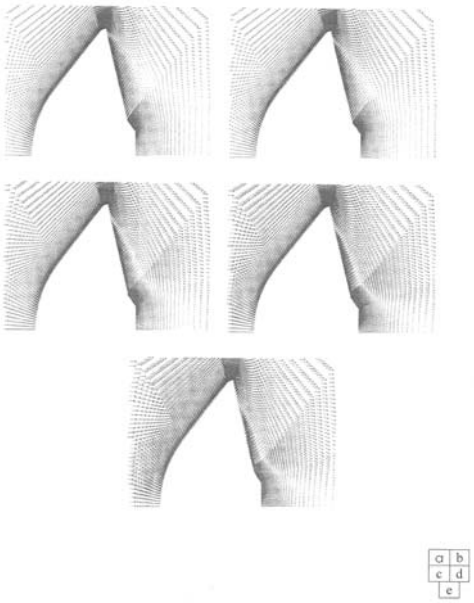

Fig.6 Close-up View of the Vector Plot over OREX Module
(a) M = 1.2 (b) M = 1.4 (c) M = 2.0 (d) M = 3.0 (e) M = 5.0

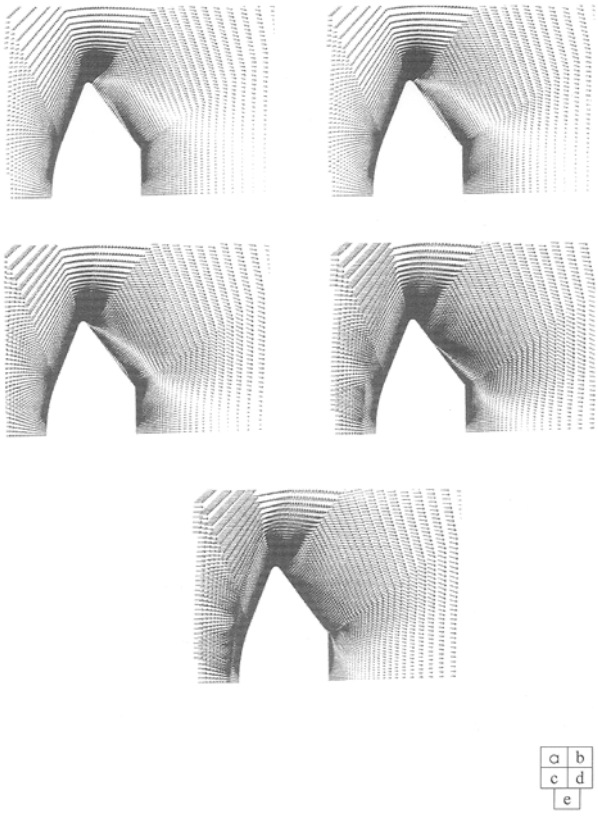

Fig.5 Close-up View of the Vector Plot over Beagle Module
(a) M = 1.2 (b) M = 1.4 (c) M = 2.0 (d) M = 3.0 (e) M = 5.0

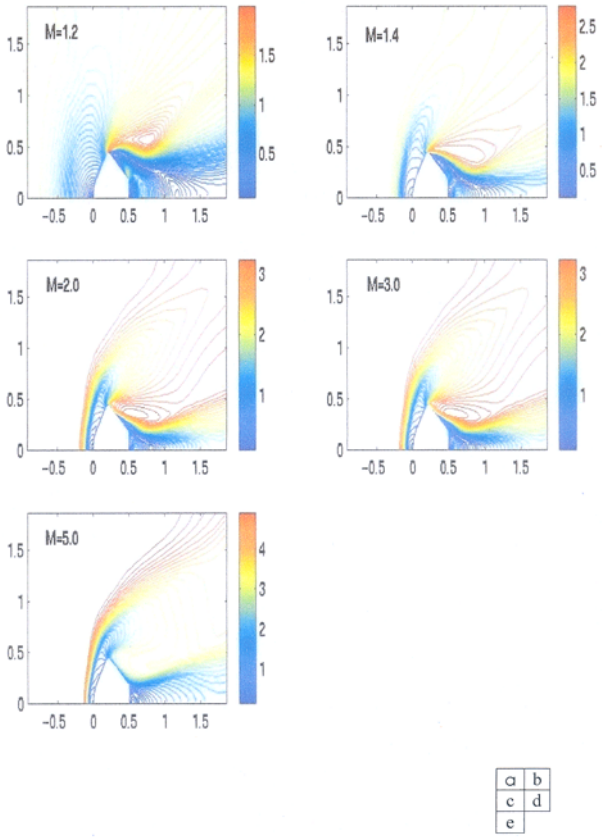

Fig.7 Mach Contour over Beagle Module
(a) M = 1.2 (b) M = 1.4 (c) M = 2.0 (d) M = 3.0 (e) M = 5.0

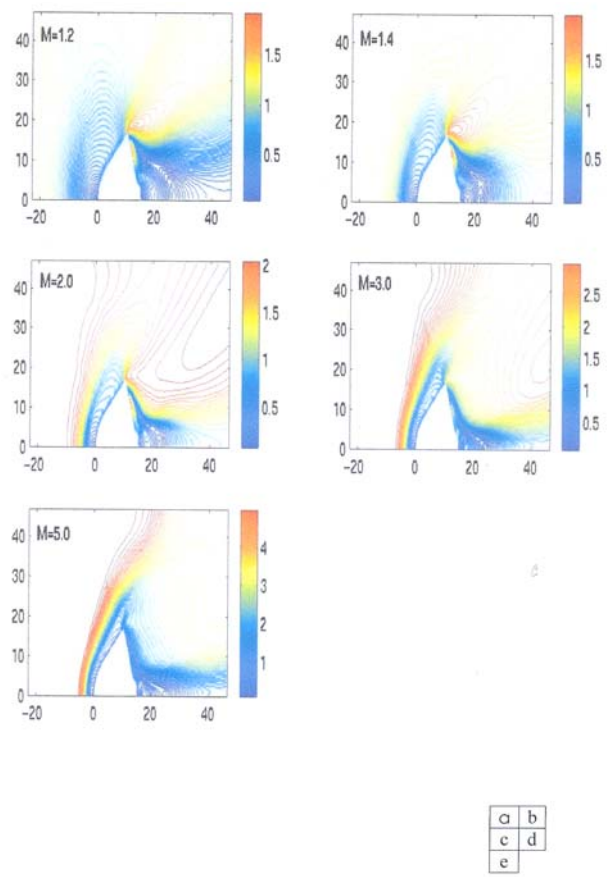

Fig.8 Mach Contour over OREX Module
(a) M = 1.2 (b) M = 1.4 (c) M = 2.0 (d) M = 3.0 (e) M = 5.0

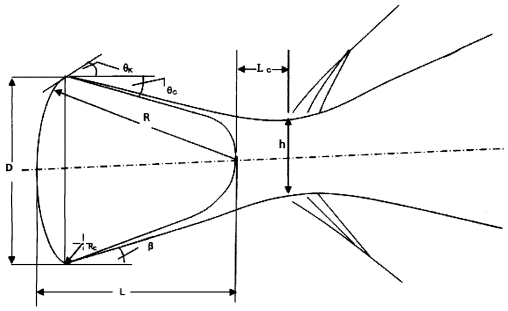

Fig.9 Presentation of Geometrical Parameters and Wake Region Flow Field

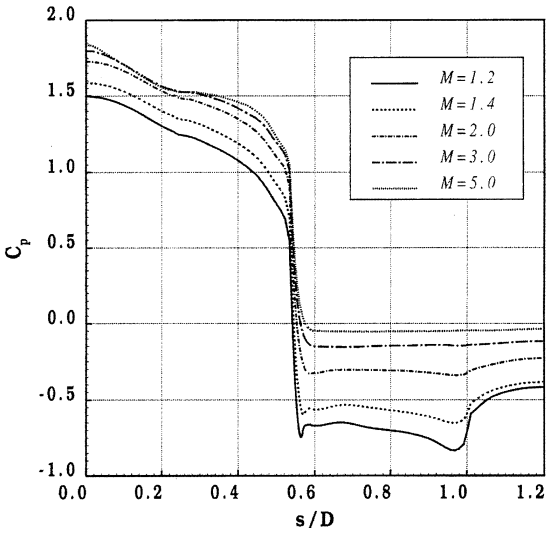

Fig.10 Variation of Pressure Coefficient along the Surface (Beagle Capsule)

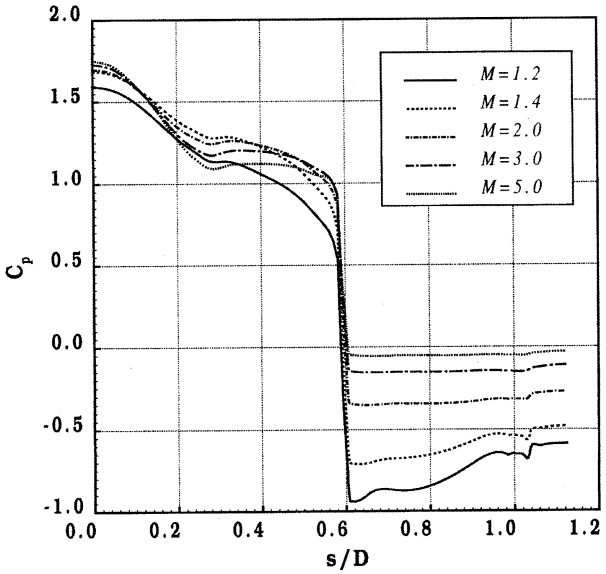

Fig.11 Variation of Pressure Coefficient along the Surface (OREX Capsule)

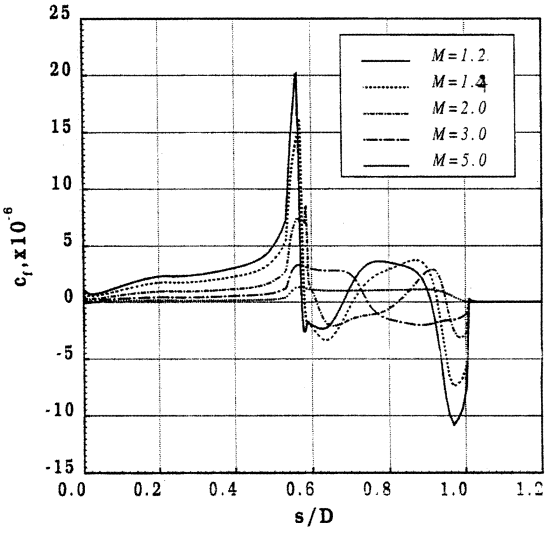

Fig.12 Variation of Skin Friction Coefficient along the Surface (Beagle Capsule)

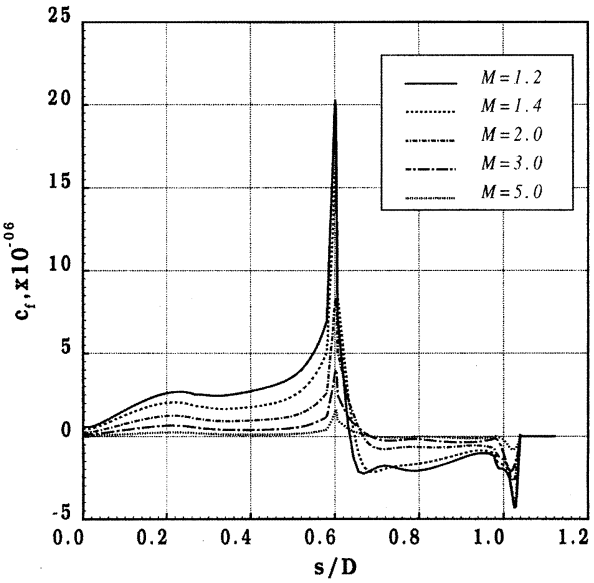

Fig.13 Variation of Skin Friction Coefficient along the Surface (OREX Capsule)

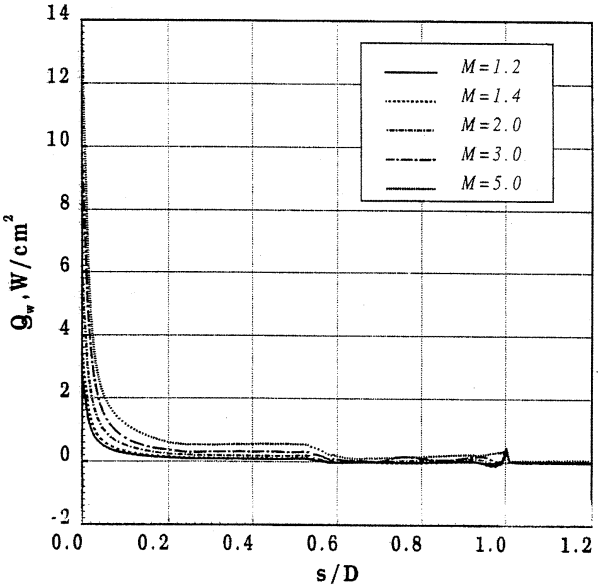

Fig.14 Variation of Wall Heat Flux along the Surface (Beagle Capsule)

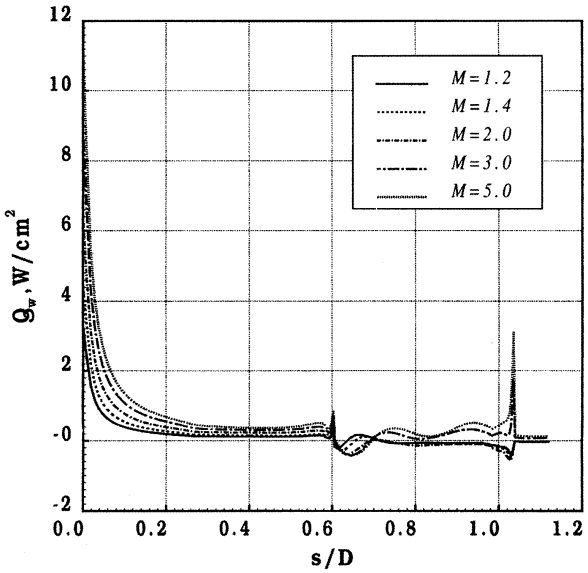

Fig.15 Variation of Wall Heat Flux along the Surface (OREX Capsule)